Climatology of the Aerosol Extinction-to-Backscatter Ratio from Sun-Photometric Measurements

Roberto Pedrós, Víctor Estellés, Michaël Sicard, José Luis Gómez-Amo, María Pilar Utrillas, José A. Martínez-Lozano, F. Rocadenbosch, C. Pérez, and José María Baldasano Recio

***Abstract*—The elastic lidar equation contains two unknown atmospheric parameters, namely, the particulate optical extinction and backscatter coefficients, which are related through the lidar ratio (i.e., the particulate-extinction-to-backscatter ratio). So far, independent inversion of the lidar signal has been carried out by means of Raman lidars (usually limited to nighttime measurements), high-spectral-resolution lidars, or scanning elastic lidars under the assumption of a homogeneously vertically stratified atmosphere. In this paper, we present a procedure to obtain the lidar ratio at 532 nm by a combined Sun-photometer–aerosol-model inversion, where the viability of the solution is largely reinforced by assimilating categorized air-mass back-trajectory information. Thus, iterative lidar-ratio tuning to reconstruct the Sun-photometric aerosol optical depth (AOD) is additionally constrained by the air-mass back trajectories provided by the hybrid single-particle Lagrangian integrated-trajectory model. The retrieved lidar ratios are validated with inversions of lidar data based on the Klett–Fernald–Sasano algorithm and with the Aerosol Robotic Network (AERONET)-retrieved lidar ratios. The estimated lidar ratios concur with the AERONET-retrieved lidar ratios and with those of the well-known KFS inversion constrained with Sun-photometric AOD values and embedded single-scattering models. The proposed method can be applied to routinely extract climatological values of the lidar ratio using measurements of direct solar irradiance (more numerous than those of sky radiance).**

***Index Terms*—Aerosols, back trajectories, extinction-to-backscatter ratio, lidar, Sun photometer.**

Manuscript received November 5, 2008; revised May 8, 2009. First published October 2, 2009; current version published December 23, 2009. This work was supported in part by the Spanish Ministry of Science and Innovation under Project CGL2007-60648 and Project CGL2009-07790); by the Spanish Commission of Science and Technology under Project CGL2005-03428-C04-01; by the European Union through the European Aerosol Research Lidar Network-Advanced Sustainable Observation System Project (EARLINET-ASOS) under Contract RICA-025991; by the European Space Agency under Contract 21487/08/NL/HE; by the European Regional Development Funds under Project TEC2006-07850/TCM; and by the Spanish Ministry of Education and Science under complementary actions CGL2008-01330-E, CGL20007-28871-E/CLI, and CGL2006-26149-E/CLI.

R. Pedrós, V. Estellés, J. L. Gómez-Amo, M. P. Utrillas, and J. A. Martínez-Lozano are with the Solar Radiation Group, Department of Earth Physics, University of Valencia, 46100 Valencia, Spain (e-mail: Roberto.Pedros@uv.es).

M. Sicard and F. Rocadenbosch are with the Remote Sensing Laboratory, Department of Signal Theory and Communications, Polytechnic University of Catalonia, 08034 Barcelona, Spain.

C. Pérez and J. M. Baldasano Recio are with the Environmental Modeling Laboratory, Earth Sciences Department, Polytechnic University of Catalonia, 08034 Barcelona, Spain.

Color versions of one or more of the figures in this paper are available online at http://ieeexplore.ieee.org.

Digital Object Identifier 10.1109/TGRS.2009.2027699

NOMENCLATURE

AERONET	Aerosol Robotic Network.
AOD	Aerosol optical depth.
ECMWF	European Centre for Medium-Range Weather Forecasts.
FNL	Final.
GDAS	Global data assimilation system.
GOME	Global Ozone Monitoring Experiment.
HYSPLIT	HYbrid Single-Particle Lagrangian Integrated Trajectory.
KFS	Klett–Fernald–Sasano.
NASA	National Aeronautics and Space Administration.
NCEP	National Centers for Environmental Prediction.
NOAA	National Oceanic and Atmospheric Administration.
OPAC	Optical Properties of Aerosols and Clouds.
TOMS	Total Ozone Mapping Spectrometer.

I. INTRODUCTION

TROPOSPHERIC aerosols play an important role in our climate because of their relation to cloud formation and sunlight attenuation. Although several models for the study of the optical properties of lower atmospheric aerosols have been developed [13], [33], [66], [70], the optical properties of particulates, governed by physical parameters such as particle density and size distribution, have not yet been well characterized. Active lidar systems contribute to the global climate effort through their ability to determine the vertical profiles of aerosol extinction and backscattering, which must be known to reduce uncertainty in the aerosol forcing of climate [31], [32]. Therefore, both elastic Raman lidars (i.e., the combination of at least one elastic channel and one Raman channel [4]) and high-spectral-resolution lidars (HSRL) [30] enable independent inversion of the particulate extinction and backscatter (and, hence, of their quotient, the so-called lidar ratio). Scanning elastic lidars can serve the purpose under the assumption of a homogenously vertically stratified atmosphere [67]. In contrast, (single-wavelength) elastic lidars using the well-known KFS inversion method (see also [23], [39], and [59]) depend on the following hypotheses or *a priori* information (for a review, see [57]):

1) A relationship between the particulate extinction and the backscatter (Mie's component). The lidar ratio is, in principle, range dependent, accounting for the different aerosol properties with range. In practice, a range-independent (i.e., a constant) lidar ratio is often used over

small range intervals or range intervals where aerosol homogeneity conditions prevail. Under these conditions, and assuming single scattering, the lidar ratio is equal to

$$LR = \frac{4\pi}{\omega_0 P_a(180^\circ)} \quad (1)$$

where ω_0 is the particulate single-scattering albedo and $P_a(180^\circ)$ is the particulate single-scattering phase function at 180° scattering angle.

2) A far-range lidar molecular calibration. This calibration is usually computed by assuming that the total atmospheric backscatter coefficient at the far-end reference range equals the molecular atmospheric backscatter level (Rayleigh's scattering) at that reference range. The backscatter coefficient is thus set at the reference altitude and supplies the boundary value required to solve the lidar equation. The backscatter coefficient is obtained by assuming only Rayleigh scattering beyond the reference altitude. In this way, the signal is normalized above the particulate layer using known Rayleigh profiles. The Rayleigh profiles can either use ECMWF forecasts [74] or an atmospheric model [69] fed with surface pressure and temperature [8]. When available, radiosonde data can be used [38]. According to Marenco *et al.* [42], this assumption is fairly realistic in the absence of clouds.

The backscatter profiles obtained from KFS inversion strongly depend on the variability of the lidar ratio (see, for example, [12], [40], and [60]). The *a priori* value of the lidar ratio is usually the largest source of systematic errors. The lidar ratio depends on two factors: humidity, which is related to height as the relative humidity increases often within the planetary boundary layer, and particulate characteristics, since it depends on the refractive index and on the size of particles [1]. Therefore, the lidar ratio can have a strong time and space variability (e.g., [1] and [26]) because changes in temperature and humidity in the atmosphere cause vertical inhomogeneity in the particulate vertical distribution [28]. Literature values of the lidar-ratio range from about 10 to 150 sr (e.g., [6], [11], [44], and [45]).

On the other hand, the retrieval of the vertical profiles of aerosol-extinction and backscatter coefficients from down-looking instruments, such as LEANDRE [24], Cloud Physics Lidar [47], GLAS [68], or CALIPSO [72], also necessitates the prescription of the lidar ratio. The accuracy of this prescribed ratio determines the accuracy of the retrieved profiles.

The necessity of a global climatology of lidar-ratio values has been pointed out by several authors [9], [11], [25]. In this paper, we present a procedure to obtain the lidar ratio at 532 nm by a combined Sun-photometer–aerosol-model inversion. The viability of the solution is supported by the use of air-mass back trajectories, which helps one to determine the aerosol model that is more representative of the atmospheric conditions. The retrieved lidar ratios concur with the AERONET-retrieved lidar ratios [17], [18] and with those of the well-known KFS lidar inversion constrained with Sun-photometric AOD values. The methodology has been applied to establish a climatology of the lidar ratio for Valencia City, a Mediterranean coastal site.

II. Instrumentation

Measurements of direct solar irradiance were made by a CIMEL CE318 photometer. This is a Sun photometer designed for automatic measurements of direct solar irradiance and sky radiance [34]. It measures in five nonpolarized channels nominally centered at 440, 670, 870, 940, and 1020 nm. The 940-nm channel is dedicated to obtaining the atmospheric columnar water vapor (CWV) [10]. The nominal full-width at half-maximum of each channel is 10 nm, and the sensor head is equipped with a double collimator with a 1.2° field of view (FOV).

Direct-Sun measurements from the CE318 photometer are used for deriving the AOD at the four aerosol channels (440, 670, 870, and 1020 nm) and the CWV with a methodology that is very similar to that of the AERONET direct-Sun-2 methodology [21]. The CE318 unit installed in Burjassot has been operating since January 2002. Since April 2007, the instrument has been included in the AERONET network.

When mineral dust is detected, further optical and radiative properties are derived by inverting the sky diffuse measurements in the almucantar planes with the ESR.pack package [21]. This package contains at its core the SKYRAD algorithm [51] in the version 4.2 currently employed by the SKYNET network [71]. The aerosol properties obtained with this code include the aerosol volume distribution, the real and imaginary parts of the refractive index, and the single scattering albedo. From the volume distribution, the package also retrieves the asymmetry parameter and the effective radius. Details about the employed methodology can be found elsewhere [22]. The application of such data for mineral dust will be discussed in Section IV-B.

In this paper, aerosol data from the CE318 unit maintained in Barcelona have also been employed. The data are the AOD, the single-scattering albedo, and the phase function at 180°, which have been downloaded from the AERONET DS2 data pool at level 1.5.

The uncertainty of calibration is a critical source of error in aerosol optical-property calculation. The progressive degradation of interference filters, caused by ultraviolet light, atmospheric humidity, extreme temperatures, and other meteorological agents, leads to a drift in time of the calibration coefficients. As the CE318 Sun photometer takes measurements of two different parameters—direct solar radiation and diffuse sky radiation—two calibrations are required. The method used and the uncertainty in the results for both direct and sky measurements are described in [21].

Another concern in the AOD validity is the presence of clouds. An automatic procedure for cloud screening was implemented in accordance with the algorithm described by Smirnov *et al.* [64]. Thin clouds, mainly high cirrus, are a real setback in Sun photometry. The cloud-screening filter tries to isolate and remove the AOD spectra that are very variable in different time intervals. In such a way, clouds are identified as they normally imprint more variable optical depths than aerosols. However, at times, high and thin stratified clouds are not variable enough and cannot be identified by the automatic algorithm. In order

to mitigate this problem, when possible, we use visual sky observation for each day and manually supervise the data using this information.

The total ozone columnar content was measured with a Microtops II portable photometer. This instrument provides the ozone content using the differential absorption method. This method requires the measurement of direct irradiance in three channels, namely, 305.5, 312.5, and 320 nm. Each of these channels has a collimator with a FOV of 2.5° and deflectors to remove internal reflections. The instrument incorporates a narrow-band interferential filter and a photodiode tailored to each band. The inaccuracy due to nonlinearity is kept below 0.002%, and the combined precision is between 1% and 2% [49]. When the Microtops II data were not available, GOME and TOMS were used. The ozone data are available on the TOMS Web site [76]. The 940-nm channel of the Microtops II photometer is used to determine the columnar water vapor. The relative humidity was obtained from meteorological stations located at the measurement sites.

The lidar-ratio output of the algorithm is validated using simultaneous lidar measurements. Prior to inverting lidar data, the range-corrected signal was visually inspected to avoid clouds. The lidar instrument was developed by the Polytechnic University of Catalonia, Barcelona, Spain. It is based on a frequency-doubled Nd:YAG laser delivering simultaneously pulses of approximately 160 mJ and 7-ns duration at 1064 and 532 nm [58]. The backscattered light is collected by an 8-in-diameter Schmidt–Cassegrain telescope and focused on one end of an optical fiber bundle. At the other end of the bundle, dichroic beamsplitters deflect the collected light toward three photodetectors. An avalanche photodiode-based receiver is used for the 1064-nm channel. A photomultiplier-tube-based receiver is used at 532 and 607.4 nm, with the latter corresponding to a Raman shift of the incident radiation at 532 nm produced by atmospheric nitrogen. The system full overlap factor is reached at 0.5 km. The lidar ratios computed from the lidar inversion are retrieved with an iterative method based on the KFS algorithm and constraining the integral over height of the aerosol-extinction coefficient profile (the lidar-derived AOD) to the Sun-photometric AOD [55]. This method requires a first-guess lidar ratio fixed to 60 sr, and by iteration on the lidar ratio, it looks for the value that allows the lidar-derived AOD to match the Sun-photometric AOD to a given uncertainty fixed by the user (0.001 here).

The Raman signals are very weak, and their extraction from the detected signal can only be performed at nighttime when the background signal is low.

Since the analysis presented in this paper is based on daytime Sun-photometric measurements, the Raman channel could not be used to retrieve the lidar ratio to validate the proposed method. The reason is that the stable atmospheric conditions are very seldom due to the strong coastal and orographic influences and the climatological settling of the Barcelona area [62]. Thus, the atmospheric conditions do not remain stable enough to consider that Sun-photometric measurements before and after a nighttime Raman lidar measurement encounter the same aerosol conditions.

III. METHOD

First, the AOD is determined by measuring the extinction of the solar direct flux with the CIMEL CE318 Sun photometer, as described in Section III-A. Next, an initial combination of basic aerosol components is selected based on the 120-h air-mass back trajectories [75], the so-called first-guess solution. The modeled AOD of such a combination of aerosol components is calculated according to the procedure described in Section III-B. The choice of the first-guess solution and the particle densities of each basic component are related to the air-mass classification discussed in Section III-D. Then, the particle densities are changed iteratively by simplex minimization of an objective function defined from the measured AOD and the modeled AOD. Section III-C details the minimization procedure. Finally, the lidar ratio of the combination of basic components is calculated using the Mie scattering model.

Sections IV-A and IV-B present the validation of the retrieved lidar ratios with inversions of lidar data based on the KFS algorithm and with the AERONET-retrieved lidar ratios. In Section IV-C, the described procedure is used to extract climatological values of the lidar ratio.

A. AOD Measured Values

The AOD is considered to be the simplest and most representative parameter for characterizing the aerosols present in the atmosphere [35]. The AOD calculation is based on the Bouguer–Lambert–Beer law, which relates the direct flux incident at ground level (F) with the extraterrestrial flux (F_0) for the aerosol channels (440, 670, 870, and 1020 nm)

$$\tau(\lambda) = \frac{-1}{m_0} \ln\left(\frac{F(\lambda)}{\rho^{-2} F_0(\lambda)}\right) \tag{2}$$

where λ is the wavelength, m_0 is the relative optical mass, ρ is the relative Sun–Earth vector, and $\tau(\lambda)$ is the total optical depth, which can be broken down into different contributions in the form of

$$\tau(\lambda) = \tau_a(\lambda) + \tau_R(\lambda) + \tau_{03}(\lambda) + \tau_w(\lambda) + \tau_{N02}(\lambda) \tag{3}$$

where $\tau_a(\lambda)$ is the AOD. $\tau_R(\lambda)$ is the molecular (or Rayleigh) optical depth (computed according to Bodhaine *et al.* [8], which includes the accurate calculation of the refractive index of air. When available, we use an experimental value of atmospheric pressure for correcting the molecular contribution. If this is not available, we rely on a standard atmosphere. $\tau_{03}(\lambda)$ is the contribution due to the optical depth due to ozone absorption, which is computed with the ozone content according to the Bouguer–Lambert–Beer law [27]. The ozone-content determination has been described in Section II; $\tau_w(\lambda)$ is the optical depth due to water-vapor absorption, which is computed by using the function proposed by Gueymard [27]. The columnar-water-vapor value required for the water optical depth is retrieved by the Microtops II Sun photometer. The Microtops II measurement relies on the application of the methodology of Bruegge *et al.* [10]. If no Microtops reading is available, a standard atmosphere value is used, although the effect of assuming

experimental or averaged values is actually very small. $\tau_{N02}(\lambda)$ is the optical depth due to nitrogen dioxide, which is computed by using a standard atmosphere value, as given in the work of Gueymard [27], for a light-polluted atmosphere. More details concerning the calculation of optical depths can be found in [20].

The Ångström exponent α is most commonly used for the qualitative description of mean particle size. The α exponent is obtained by fitting the measured AOD in the channels of 440, 670, 870, and 1020 nm, according to Ångström's formula [3], [43]

$$\tau_a(\lambda) = \frac{\kappa}{\lambda^\alpha} \tag{4}$$

with κ being the AOD at 1 μm. The α exponent determines the slope of the curve of the spectral dependence of the AOD. Smaller particles are characterized by a more marked spectral dependence and, therefore, a greater value of α than for larger particles, whose optical depth is far less spectrally dependent. This fact will be used to explain the behavior of the AOD inversion for dust.

The uncertainty associated with the measurement of the AOD was calculated by using the well-known error propagation method [21], using as primary sources of noise the instrument calibration, the optical mass calculation, and the error due to the optical-depth determination of the rest of the atmospheric components in (3). The calculated uncertainty is on the same order as the nominal uncertainty of AERONET (0.01–0.02) [19].

B. AOD Modeled Values

The AOD is calculated by integrating the extinction coefficient of a composite aerosol model over the whole atmospheric column. The composite aerosol model is a combination of several basic components, whose optical properties have been computed by Hess *et al.* [33] by means of Mie scattering theory. These properties include, for each basic aerosol component, the refractive index, as well as the following aerosol distribution parameters: the mode radii for several relative humidity values, and the standard deviation of the lognormal size distribution shown in

$$n_i(r) = \frac{N_i}{\sqrt{2\pi}\, r \ln \sigma_i} \exp\left[\frac{1}{2}\left(\frac{\ln r - \ln r_{\mathrm{mod},i}}{\ln \sigma_i}\right)^2\right] \tag{5}$$

where the i index numbers the basic aerosol components, r is the aerosol radius, $r_{\mathrm{mod,i}}$ is the modal radius, N_i is the particle density, and σ_i is the standard deviation. The aforementioned basic aerosol components used in our approach are water-insoluble particles, water-soluble particles, soot, sea salt, and transported mineral dust. As a simplification, we assume that the aerosols are in external mixture, i.e., there is no physical or chemical interaction between particles of different components that constitute the aerosol composite [33]. The extinction coefficient of the aerosol composite is calculated as a linear combination of the extinction coefficients of the basic components (using for water-soluble particles and sea salt the mode radii at the measured relative humidity) weighted by their respective particle densities. Finally, the AOD is calculated by integrating the extinction coefficient over the whole atmospheric column.

The described method aims at climatological values of the lidar-ratio constant for the whole atmospheric column. This makes the aerosol-extinction vertical distribution not relevant in our study, as we focus in the extinction integrated in height, i.e., the AOD, regardless of how the aerosols are actually distributed. Thus, we can assume that the aerosol-extinction vertical distribution follows an exponential profile [61] with layer depths and scale heights taken from Hess *et al.* [33] and Holzer-Popp *et al.* [36]. The drawback of using exponential profiles is that the retrieved lidar ratios can be applied to process monochromatic lidar signals only when a single aerosol layer is detected, assuming that the aerosols are well mixed.

C. AOD Inversion and Determination of the Lidar Ratio

The determination of the lidar ratio is based on iteratively reconstructing the AOD determined from Sun-photometric measurements, which will be hereinafter referred to as combined Sun-photometer–aerosol-model inversion. For a chosen combination of basic aerosol components, i.e., a linear combination of lognormal size distributions, as shown in (5), the particle densities N_i are changed iteratively until the AOD modeled values and the AOD measured values match within $\pm 5\%$ at the most [53]. The selection of appropriate basic components is discussed in Section III-D. The objective function F that is minimized is the norm of the resulting vector of subtracting the measured and modeled AOD vectors

$$F = \|\overrightarrow{\mathrm{AOD}}_{\mathrm{measured}} - \overrightarrow{\mathrm{AOD}}_{\mathrm{modeled}}\| \tag{6}$$

where the vector components correspond to the wavelengths of the Sun-photometric measurement. The F function is minimized by varying iteratively the particle densities of the chosen basic aerosol components using the Nelder–Mead simplex minimization method [52]. Nevertheless, the solution is not necessarily unique, as several combinations of basic aerosol components and particle densities might lead to the same AOD. Furthermore, the inversion shows a strong bias due to the first-guess solution. *A priori* information on the origin and type of air mass reaching the study zone can provide a reasonable first-guess solution. This solution is an initial combination of basic aerosol components selected according to the 120-h air-mass back trajectories [75]. The first-guess solution constrains the inversion by selecting only one or, occasionally, two combinations of basic aerosol components and excluding the remaining possibilities. Thus, the use of back trajectories synergetically contributes in finding a unique combination of components closer to reality. More details are given in Section III-D.

The lidar ratio is calculated by using the OPAC aerosol model using as input parameters the combination of basic aerosol components and their corresponding particle densities that minimized the objective function in (6). The extinction efficiency $Q_{\mathrm{ext}}(r, m_i, \lambda)$, the backscatter efficiency $Q_{\mathrm{back}}(r, m_i, \lambda)$, and

the lognormal size distribution $n_i(r)$ are used in (7) to compute the lidar ratio

$$LR = \frac{\sum_{i=1}^{M} \int_0^{\infty} Q_{\text{ext}}(r, m_i, \lambda)\pi r^2 n_i(r)\, dr}{\sum_{i=1}^{M} \int_0^{\infty} Q_{\text{back}}(r, m_i, \lambda)\pi r^2 n_i(r)\, dr} \tag{7}$$

where M is the total number of basic aerosol components i and m is the refractive index.

D. Air-Mass Classification

Knowledge of the origin of the air masses provides *a priori* information that helps one to establish a realistic first-guess solution for the minimization of the objective function in (6). This information consists of a plausible combination of basic aerosol components based on aerosol models by Hess *et al.* [33] and Holzer-Popp *et al.* [36] and associated to the air-mass classification proposed by Estellés *et al.* [22]. This most plausible combination of basic aerosol components in the first guess increases the viability of the solution.

Air masses can be classified, with respect to the source region, in terms of two parameters: temperature and surface type. Temperature allows a distinction to be made between Arctic, Midlatitude, and Tropical situations, depending on the latitude where the air masses originated. On the other hand, the surface type of the region may be continental or maritime, depending on whether they have been developed over continental or oceanic surfaces, respectively [7]. The classification method proposed by Estellés *et al.* [22] was based on the following: 1) a sectorization of the surrounding source regions; 2) a model for computation of the air-mass origin and history path; and 3) a set of rules for determination of the air-mass character. The paths followed by the air masses were given by their 120-h back trajectories at different levels, computed with the NOAA HYSPLIT, which is one of the most used models. Back-trajectory computation is available online [75] and uses the $1^\circ \times 1^\circ$ latitude–longitude grid, FNL meteorological database [15]. The 6-h FNL archived data are generated by NCEP's GDAS wind-field reanalysis. GDAS uses the spectral medium-range forecast model for the forecast. The FNL database contains basic meteorological parameters, such as the horizontal-wind components, temperature, and humidity at 13 different levels, from a surface level up to 20 hPa. For each day, three back trajectories were calculated simultaneously, starting at different altitudes above the measurement station: 1) 500 m above sea level, well within the boundary layer where a greater part of the interactions affecting the aerosols occur, although these same interactions create the greatest uncertainty in the back trajectory; 2) 1500 m above sea level trying to represent the top of the nominal boundary layer; and finally, 3) 3000 m above sea level, representing the free troposphere, which has been observed to ubiquitously contain organic aerosols [29], [54] and also, although relatively less frequent, mineral dust [56].

For the sectorization, Estellés *et al.* [22] defined $5 + 1$ sectors for Valencia City, a Mediterranean coastal site. Fig. 1 shows

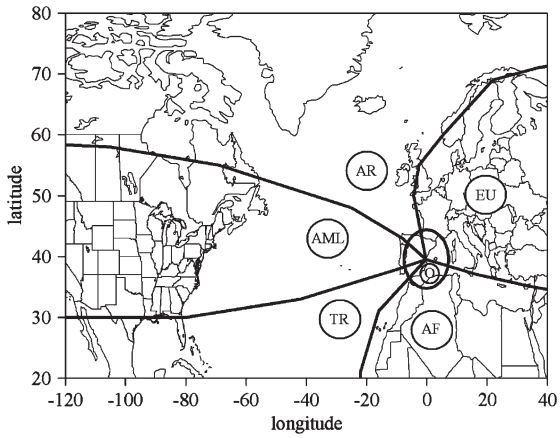

Fig. 1. Air-mass classification into five predominant classes for a Mediterranean coastal site Burjassot (Spain).

the sectors used for classifying the arriving air masses. The sectors are as follows: European, African, Tropical, Atlantic Midlatitude, Arctic, and Regional. The defined sectors and mean aerosol size distributions appear in [22].

EU Sector (European): This sector defines continental midlatitude air masses from Europe. Its differential characteristic is the urban-type aerosol load, including smoke and soot. The mean size distribution is characterized by a well-developed accumulation mode and a relatively low single-scattering albedo, with high variable AOD and Ångström wavelength exponent. The air mass comes from northern Finland and crosses the European continent before reaching the city of Valencia. The first guess associated to this sector is the continental combination of basic components: water-insoluble particles, water-soluble particles, and soot [33].

AF Sector (African): The AF sector is characterized by tropical continental air masses. The air masses have a variable load of mineral dust due to the Sahara desert and the low-pressure cells that arise from the high levels of solar irradiance in summer. This causes dust to be injected at elevated layers and transported to other latitudes. The air masses are strongly turbid, thus with high AOD. The aerosols are described by a low Ångström wavelength exponent, and thus, the size distribution has a dominant coarse mode. For this sector, the first guess would be the mineral-dust combination of components: water-soluble particles and transported mineral [36].

TR Sector (Tropical): The Atlantic Ocean has been divided into three regions. The first one corresponds to tropical maritime air masses in western Africa. The air masses possess a certain mineral footprint. Turbidity is higher than the other two Atlantic regions although lower than the pure AF class. In the size distribution, the coarse mode was found to be dominant.

AML Sector (Atlantic Midlatitude): This is the region of the Atlantic located between average latitudes (between 30° and 60°). These were midlatitude maritime air masses generated by the movement of continental air masses from North America.

AR Sector (Arctic): AR Sector (Arctic) defines air masses that originate in Canada or in the Arctic basin, with associated air masses of type Arctic maritime or midlatitude maritime, according to the exact place of origin. AML and AR air masses are the cleanest cases with variable Ångström exponent and

size distribution with low modes [22]. For the three sectors TR, AML, and AR, the first guess would be the maritime typified distribution or a mixture of continental and maritime. The reason for this mixture is that the Atlantic air masses have to cross the Iberian Peninsula before arriving at the site, possibly being loaded with continental aerosols as a result. For the maritime composite, we will use the following basic components: water-soluble particles, soot, and sea salt (both in accumulation and coarse modes), based on the work of Hess *et al.* [33]. The mixture of continental and maritime is formed by adding the insoluble component to the maritime combination, so the resulting composite will have both maritime and continental basic components (thus, water-insoluble particles, water-soluble particles, soot, and sea salt in accumulation mode and sea salt in coarse mode). Both combinations of components are examined because we are not certain of which is the dominant one. The best combination of components reproducing the measured AOD is taken as the most representative of the aerosol distribution.

An Auxiliary Regional class (O) was defined to account for the stationary air masses wandering around the final destination. Sector O corresponds to synoptic situations of weak pressure gradients causing air masses to travel a maximum distance of 600 km over the last five days, usually crossing several sectors. This sector seldom appears, but it has been included for thoroughness. For this sector, a first guess is not possible, so all the aforementioned combinations of basic components are examined to minimize the objective function in (6). For those cases, when it is not possible to determine which sector is predominant between the two, the first-guess combination of basic components of each sector is examined. The one that presents a minimum objective function is selected.

IV. Results

A two-year database has been used to validate the combined Sun-photometer–aerosol-model inversion with lidar ratios based on the KFS lidar inversion and with the AERONET-retrieved lidar ratios. The AOD inversion is then applied to obtain a climatology of the lidar ratio in a Mediterranean coastal site.

A. Uncertainty Estimates of the Retrieved Lidar Ratios

For the combined Sun-photometer–aerosol-model inversion, the uncertainty of the lidar ratio is computed by using the well-known error-propagation method. Specifically, this is the quadratic sum of two terms: 1) the uncertainty that arises from the inversion in the form of the root-mean-square value of the residuals after minimizing the objective function in (6) and 2) the uncertainty associated with AOD retrieval from Sun-photometric data in the range of 0.01–0.02 [22]. For the set of data used, a worst case estimate of the uncertainty is 20%.

For the AERONET-inversion, the possible errors in instrument and inversion cannot be computed analytically to furnish an uncertainty estimate in the retrieved lidar ratios [16]. Nevertheless, Cattrall *et al.* [11] state that the uncertainties are not high, although they rather use the standard deviation of a Gaussian fit as an indicator.

TABLE I
EXAMPLE OF LIDAR-RATIO VALUES (IN STEREORADIANS) AT 532 nm FOR THE MOST TYPICAL AEROSOL TYPES AND AIR MASSES. THE UNCERTAINTY OF THE LIDAR-RATIO ESTIMATES ARE AS FOLLOWS: AOD INVERSION: 20%; AERONET INVERSION: CANNOT BE COMPUTED ANALYTICALLY (SEE THE TEXT FOR MORE DETAILS); LIDAR INVERSION: 10%

Aerosol Type	AOD inversion	AERONET inversion	Lidar inversion
Continental (*European*)	60	61	63
Continental (*Regional*)	59	75	66
Mixture continental + maritime (*Atlantic – Arctic*)	35	45	36
Mineral dust outbreak (*African*)	55	55	60

According to Pelon *et al.* [55], the uncertainty of the KFS-retrieved lidar ratio is the quadratic sum of two terms: 1) the uncertainty resulting from the natural variability associated with the data, which is calculated as the standard deviation of the lidar ratio computed for each individual profile, and 2) the uncertainty associated with the uncertainty on the AOD, i.e., 0.01–0.02 [22]. For the set of data considered in this paper, a worst case estimate of the uncertainty associated with the lidar ratio is 10%.

B. Validation

We have compared the lidar-ratio outputs of the combined Sun-photometer–aerosol-model inversion at 532 nm with the lidar ratios computed from the lidar inversion based on the KFS algorithm considering a constant lidar ratio. The AOD-inverted lidar ratios have also been compared with those obtained from AERONET aerosol inversions. The database covers the years 2007 and 2008 and has been selected so that measurements of direct solar irradiance, sky radiance, and lidar profiles are made with less than 1-h difference. The simultaneity is very demanding and has reduced the two-year database to 26 days of measurement. The AERONET aerosol inversions (level 1.5) provide the single-scattering albedo and the phase function at 180°, which are used to calculate the lidar ratio at 532 nm by using (1) and a cubic-spline interpolation (which will be hereinafter referred to as AERONET-inverted lidar ratio).

Table I shows the lidar-ratio estimates derived from single instances (i.e., as in Fig. 2) of the most typical aerosol types and air-mass origins in the Iberian Peninsula (continental, maritime, and mineral-dust intrusion) using each of the three different retrieval techniques. The air-mass origins appear in Fig. 2, which contains the 120-h signature previous to the start of the Sun-photometric measurements. The study site is Barcelona (Spain), a Mediterranean coastal site. Barcelona is about 300 km north of Valencia, the site used in the air-mass classification described in Section III-D. Since both cities are not far apart from each other compared to the distances traveled by the air masses, the air-mass classification can be applied to Barcelona.

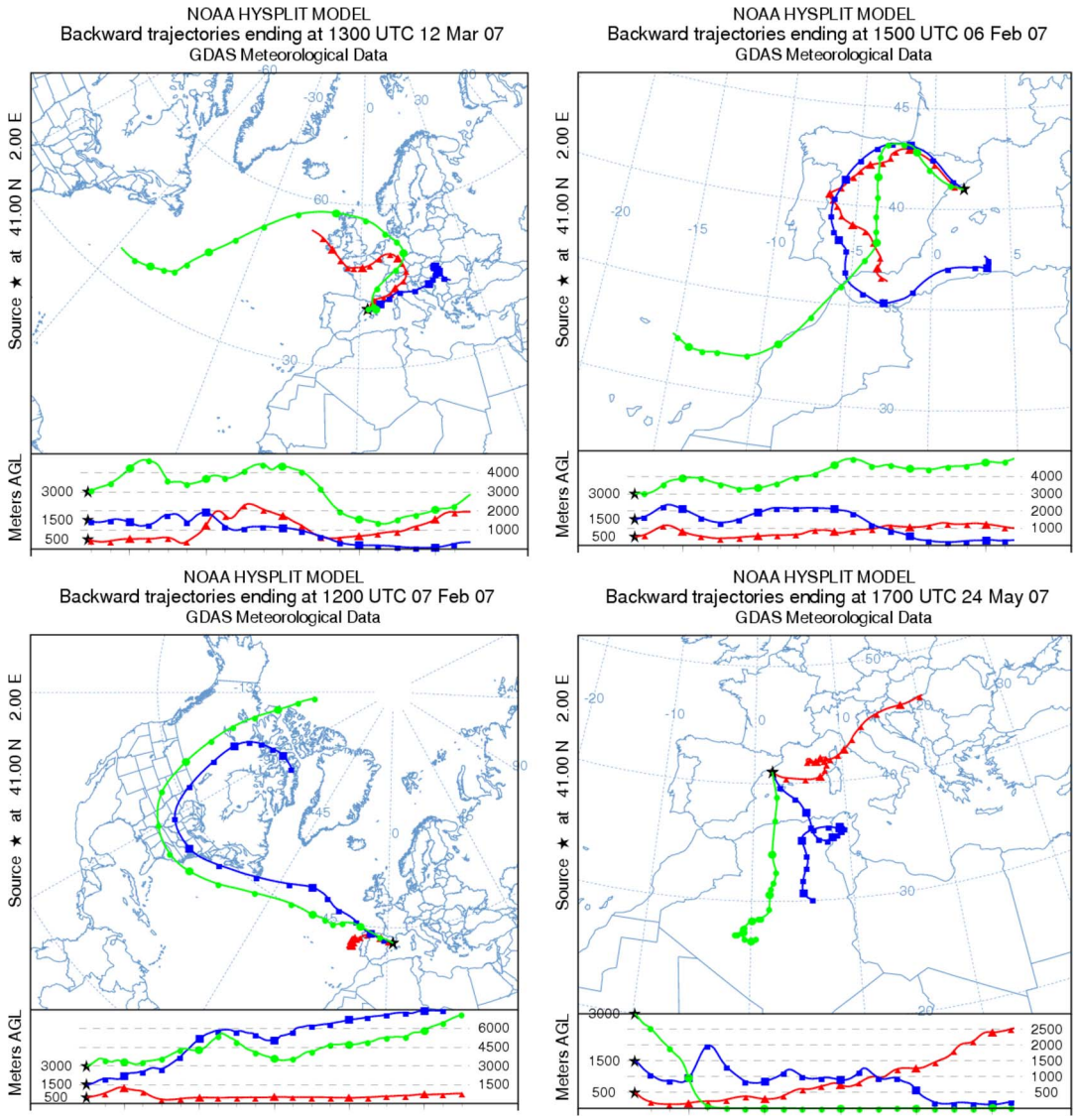

Fig. 2. As computed with the NOAA HYSPLIT model ending in Barcelona, these are 120-h air-mass back trajectories. (a) Continental aerosols on March 12, 2007, at 13:00 UTC from the European sector. (b) Continental aerosols on February 6, 2007, at 15:00 UTC from the Regional sector. (c) Maritime aerosols on February 7, 2007, at 12:00 UTC from the Arctic sector. (d) Mineral-dust outbreak on May 24, 2007, at 17:00 UTC from the African sector.

Furthermore, both cities exhibit very similar characteristics as Mediterranean coastal sites in densely populated areas, so the results can reasonably be extrapolated from one to the other.

In Fig. 2(a), the air masses are in the EU sector, so according to Section III-D, the first guess for the minimization of (6) is the continental combination of basic components. For Fig. 2(b), the air masses correspond to the Regional class. In this case, the best results of the AOD inversion correspond to continental aerosols. Fig. 2(c) shows an AR air-mass class, i.e., the air masses have spent part of the previous 120 h over the Atlantic Ocean, but they have also crossed the Iberian Peninsula. Therefore, both the maritime composite and the mixture of maritime and continental are examined in the minimization of (6). Fig. 2(d) shows a clear passage of the air masses over the Sahara region at high altitude. The air masses are classified into the AF sector, and we can reasonably assume that Saharan dust is the dominant type in elevated layers. This is supported by a measured AOD that is relatively high, i.e., 0.26 at 675 nm, and a low value of 0.42 of the fitted Ångström exponent α, which indicates the addition of large particles to the atmospheric column. This Saharan outbreak could be described as the linear combination of water-soluble particles and transported mineral according to Section III-D.

For the situation of Fig. 2(a), the continental aerosols issued from the combined Sun-photometer–aerosol-model algorithm (AOD inversion) yield a lidar ratio of 60 sr. This value concurs with the lidar ratio of 63 sr resulting from the KFS inversion of the simultaneous lidar measurements. The AERONET-inverted lidar ratio for this case is also very similar, with a value of 61 sr. The Sun-photometer–aerosol-model-algorithm lidar ratios are also coherent with several values found in the literature: the values of 60–70 sr with a 20% uncertainty for continental aerosols [14], and with the value of 64 ± 4 sr for a continental site [2], both measured with a 180° backscatter nephelometer, as well as with the values measured with a Raman lidar in the range of 30–80 sr by Ansmann *et al.* [5] for polluted continental

air and between 60 and 70 sr for the urban aerosols measured [45]. Cattrall *et al.* [11] determined from AERONET data an average value of 71 $\pm$ 10 sr for urban/industrial aerosols.

Fig. 2(b) corresponds to continental aerosols in the Regional class, which indicate weak pressure gradients and, thus, stationary air masses. The combined Sun-photometer–aerosol-model algorithm gives a lidar ratio of 59 sr. This value fits within the uncertainty range with the lidar ratio of 66 sr from the KFS inversion of the lidar measurements. The AERONET inversion gives a lidar ratio of 75 sr, thus deviating 13% from the lidar-inverted value and comparable to the 11% deviation of the AOD-inverted lidar ratio with the lidar-inverted value.

With regard to the Atlantic air masses in Fig. 2(c), we have assumed the following: 1) maritime aerosol and retrieved a lidar ratio of 39 sr; 2) a mixture of continental and maritime and retrieved a lidar ratio of 35 sr, with also the best result in the minimization of the objective function. These results, particularly the mixture of maritime and continental, concur with the value of 36 sr of the KFS lidar inversion. However, the AERONET inversion gives a value of 45 sr, which deviates almost 30% from the AOD-inverted value. This Atlantic air mass has a low AOD of 0.08 at 675 nm. Thus, this quite-clean air mass is likely increasing the relative error in the retrieval of the lidar ratio in the AERONET inversion. On the other hand, the lidar ratios retrieved with the AOD inversion are also consistent with the values around 40 sr obtained by Ansmann *et al.* [5] with a Raman lidar for mixtures of maritime and continental aerosols. The lidar ratio for maritime aerosols is lower than this value, so it probably yields an underestimated result. For instance, Doherty *et al.* [14] measured values around 20 sr, with an uncertainty of 20% with a backscatter nephelometer; Müller *et al.* [50] found an average of 23 $\pm$ 3 sr for North Atlantic maritime aerosols with a Raman lidar. Also, [11] obtained an average lidar ratio for oceanic aerosols of 28 $\pm$ 5 sr with AERONET.

With regard to the mineral-dust outbreak in Fig. 2(d), the combined Sun-photometer–aerosol-model inversion initially yields a lidar ratio of 27 sr, and the KFS lidar inversion gives a value of 60 sr. Lidar ratios of mineral dust can vary strongly as a function of size distribution, particle shape, and particle chemical composition, i.e., content of light-absorbing hematite [50]. Ackermann *et al.* [1] computed lidar ratios around 20 sr by assuming spherical shape of the dust particles. Barnaba and Gobbi [6] computed with an aerosol model 532-nm lidar ratios and found values between 35 and 50 sr under the assumption of spheroid-like particles. Liu *et al.* [41] obtained values between 13 and 39 sr using a spherical model and between 21 and 60 sr using T-matrix calculations applied to oblate and prolate spheroids. Values measured using HSRL and Raman range between 42 and 55 sr, with a mean of 51 sr. However, Liu *et al.* examined Asian dust, which may not be directly comparable to the Saharan dust present in the Mediterranean. Mattis *et al.* [46] clearly showed the impact of dust shape on reducing the backscatter coefficient, whereas the light extinction remained fairly constant. Mattis *et al.* found values of lidar ratios between 50 and 80 sr with a Raman lidar and explained them by considering dust as nonspherical particles, a fact that had been predicted by Mishchenko *et al.* [48]. Cattrall *et al.* [11] determined lidar

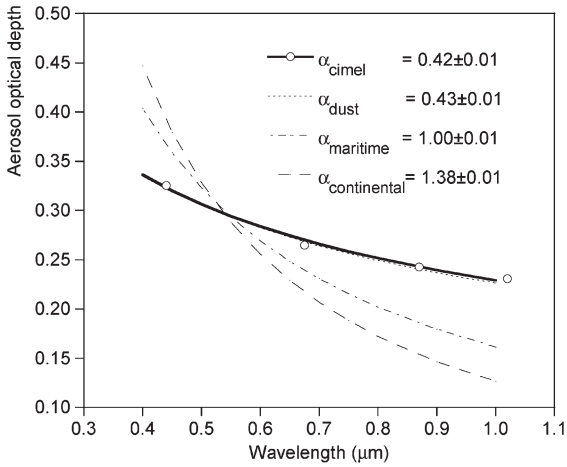

Fig. 3. Measured (circles) and modeled AODs using Mie scattering theory for continental and maritime aerosols and mineral dust. Ångström parameter α fitting of AOD according to (4). Barcelona (Spain) on May 24, 2007, at 17:17 UTC.

ratios of 15 $\pm$ 2 sr for dust (considering spherical particles) and 42 $\pm$ 4 sr for dust (for spheroids). For the Fig. 2(d) case, the lidar-inverted lidar ratios concur with the values reported for mineral dust. In some other cases, the lidar-inverted lidar ratios presented large discrepancies with the directly measured lidar ratios found in the literature. This can be attributed to the limitations of the inversion method, particularly the use of only one elastic wavelength and the consideration of single scattering in the lidar equation. These inversions were discarded.

Although the combined Sun-photometer–aerosol-model inversion considers that aerosols are spherical, mineral dust is the composite that minimizes the objective function in (6). The reason for the agreement is the low Ångström coefficient α, i.e., the smaller slope in the curve of AOD as a function of wavelength of the mineral-dust composite. Fig. 3 shows the measured and modeled AODs for continental and maritime aerosols and mineral dust. The Ångström exponent α of the measured AOD is 0.42 $\pm$ 0.01. Mineral dust is the combination that best fits the measured AOD, having a value of α of 0.43 $\pm$ 0.01. On the other hand, continental and maritime exhibit a poor fit as the Ångström exponents α's are much higher (1.38 $\pm$ 0.01 and 1.00 $\pm$ 0.01, respectively) than that of the measured AOD. Nevertheless, the fact that the OPAC model uses spherical particles may lead to underestimate the lidar ratio for mineral dust [6]. Thus, when mineral dust is the combination of aerosol basic components that minimizes the objective function in (6), we suggest the use of the latest state-of-the-art computation values for spheroid-like particle shapes by Dubovik *et al.* [18] for several radius values, rather than sticking to the Mie output lidar-ratio values. These computed lidar ratios are about 70 sr (for a radius r_{v} of 5 μm), 55 sr (for 2 μm), and 45 sr (for 1 μm). The AERONET aerosol inversions (available on the AERONET homepage [73]) will provide the radius of the size distribution to select the appropriate lidar ratio for each dust situation. For the mineral-dust outbreak shown in Fig. 2(d), the size-distribution inversion shows a coarse mode around 2 μm at the time of the measurement. Therefore, according to Dubovik *et al.* [18], the corresponding lidar ratio would be 55 sr.

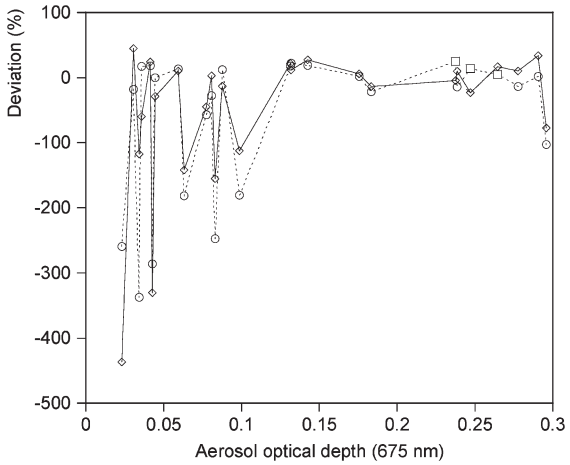

Fig. 4. Deviation of the lidar ratio at 532 nm derived from (straight line) the AOD inversion and from (dotted line) the AERONET inversion with respect to the KFS lidar inversion. Mineral dust is marked as squares.

Fig. 4 shows the results of the deviations of the lidar ratios of the AOD inversion and the AERONET inversion with respect to the KFS lidar inversion. For the AOD at 675 nm below 0.1, the deviations are large. One cause is that low AOD values make the AERONET inversion less reliable. Also, many low AOD cases appear in winter when boundary-layer heights are about 1 km. In these cases, the fact that the full overlap of the lidar is 0.5 km leads to errors in the lidar inversion. On the contrary, for larger AOD values, the deviations with respect to the KFS-inverted lidar ratios are smaller, with an average deviation for both procedures of $\pm 21\%$ and similar tendencies.

We have also analyzed the deviations of the AOD-inverted lidar ratios with respect to the AERONET-inverted lidar ratios for the whole 2007–2008 AERONET database, i.e., without the restriction of temporal coincidence with lidar measurements. The differences of the combined sun photometer–aerosol-model inversion with respect to the AERONET-inverted lidar ratios are $\pm 21\%$ for AOD at 675 nm above 0.1. This value is consistent with the uncertainty estimate of the lidar ratio for the proposed method.

C. Multiannual Climatology of the Lidar Ratio

We have applied the procedure described in Section III to a database of continuous measurements carried out with a CIMEL Sun photometer from June 6, 2003, to July 30, 2005. The site of measurements is Burjassot, which is located in the metropolitan area of Valencia (39.5° N, 0.4° W), a Mediterranean coastal site. After filtering cloudy days and only selecting the data with available relative humidity, the database was reduced to 545 days of measurement. HYSPLIT air-mass back trajectories were obtained for the entire database.

Fig. 5 shows the daily cases of the incidence of each pure and several mixed air-mass types with sufficient number of cases for our study to be relevant. The air masses that were most frequently found were of AF class and mixed AML–TR type. The histogram also shows the minimal incidence of the mixed TR–AF class. Some 7% of the days are sectors, or combinations of sectors, with low occurrence, which have not been included in the analysis of the lidar ratio.

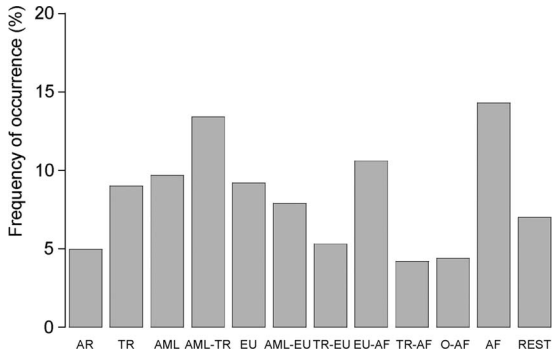

Fig. 5. Incidence of each type of air mass in Valencia City during the period considered. AF: African. TR: Tropical. EU: European. AML: Atlantic Midlatitude. AR: Arctic. O: Auxiliary Regional class.

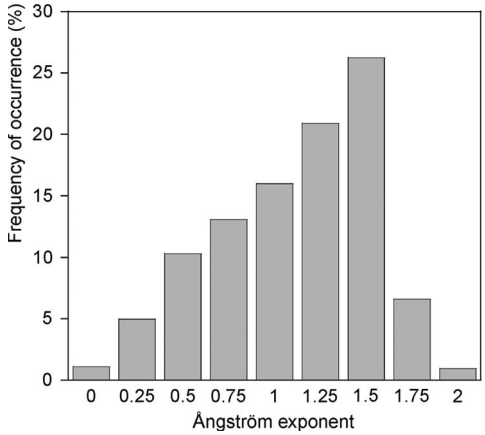

Fig. 6. Frequency histogram for the Ångström parameter α (440–1020 nm) at Burjassot.

The AOD inversion shows that continental aerosols appear on 42% of the days, for which the mean lidar ratio is 62 ± 13 sr. For coastal sites, the Ångström exponent α is expected to have higher values than those reported for remote maritime sites. These higher α values are related to background conditions, i.e., the mixture of maritime aerosols, typical of coastal sites, with continental or urban-polluted aerosols [65]. The frequency histogram of α shown in Fig. 6 shows only one frequency mode, centered at 1.5, which coincides with the mean α for continental aerosols. Maritime aerosols appear on 38% of the days and have a mean lidar ratio of 37 ± 10 sr. The mean α for maritime aerosols is 1.21, which accounts for the occurrences of α around 1.0 in Fig. 6. The background conditions also account for the α value of 1.18 for the mixture of continental and maritime. Such a mixture appears only on 7% of the days, which yield a mean lidar ratio of 33 ± 17 sr. Saharan dust intrusions are not rare, appearing on 13% of the days. Since the AERONET inversions were not available, we have inverted the sky-radiance data with the ESR.pack package to obtain the radius of the coarse mode in the size distribution. These radii were used to replace the underestimated Mie output lidar ratios by using the computations by Dubovik *et al.* [18].

The mean lidar ratio of mineral dust is 51 ± 3 sr due to a higher proportion of radius in the coarse mode of 2 μm [18]. The mean value of α for mineral dust is 0.60. This low value is the result of the extinction by large particles that constitute the dust [37], [63]. The α values that are greater than 1.75 in Fig. 6,

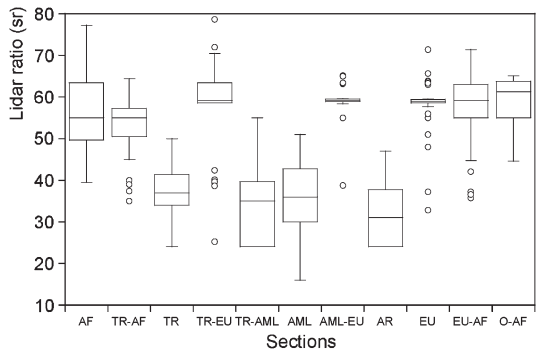

Fig. 7. Lidar ratio at 532 nm, as derived from the AOD inversion for each relevant air-mass section abscissa. AF: African. TR: Tropical. EU: European. AML: Atlantic Midlatitude. AR: Arctic. O: Auxiliary Regional class.

which also have a low mean AOD value of 0.1, correspond to forest fires.

Fig. 7 shows a climatology of the lidar ratios according to the air-mass sector or combination of two sectors. In this box diagram, the divisory segment in the box represents the median; the top (bottom) box limits represents the upper (lower) quartile—UQ (LQ). The difference between UQ and LQ is the interquartile distance (IQD). The circles are the outlier points, whose value is either greater than UQ + 1.5 IQD or less than LQ − 1.5 IQD; the top whisker (a vertical line ending in a capital T) is the largest value that is not an outlier; the bottom whisker (a vertical line ending in an inverted capital T) is the lowest value that is not an outlier.

Due to the differences in the lidar-ratio values that may appear in the same sector, we use the median values for the analysis, as they provide a more representative lidar ratio than the mean. The EU sector is dominated by continental aerosols with 88% of the cases, and thus, the median lidar ratio is 59 ± 11 sr. The AF sector has an equal occurrence of 44% for both continental and mineral-dust outbreak, as well as 12% for maritime and a mixture of continental and maritime aerosols. This accounts for the median value of 55 ± 5 sr. On 44% of the days, aerosols are dust, 56% of which have a radius for the coarse mode of 2 μm; and on 12% of the days, aerosols are maritime pure or mixture with a median lidar ratio of 41 ± 4 sr. On the other hand, the three Atlantic sectors AML, AR, and TR exhibit similar features. Maritime aerosols constitute the more typical situation occurring in more than 80% of the cases. Thus, the median values are 36 ± 11 sr for AML, 31 ± 11 sr for AR, and 37 ± 9 sr for TR.

With regard to the mixed sectors, TR–AF has a median lidar ratio of 55 ± 7 sr. This value corresponds to 30% of the days with maritime pure and mixture with continental aerosols, and 43% of the days with mineral dust, 80% of which have a particle radius of 2 μm. Sector TR–EU has a lidar ratio of 59 ± 13 sr, as it is dominated by continental aerosols on nearly 80% of the days. Similarly, section AML–EU is also dominated by continental aerosols, leading to a lidar ratio of 59 ± 11 sr. On the contrary, the TR–AML sector exhibits a lidar ratio of 35 ± 11 sr, which corresponds to more than 80% of maritime pure aerosols. With regard to section O–AF, continental aerosols account for 71% of the days, as opposed to 21% of mineral dust, leading to a median lidar ratio of 61 ± 6 sr.

V. Conclusion

We have obtained the lidar ratio at 532 nm for a multiannual database of continuous Sun-photometric measurements of direct irradiance at a Mediterranean coastal site. The method is based on reconstructing the AOD determined from Sun-photometric measurements by iterative lidar-ratio tuning. An air-mass back-trajectory classification is used to help in the selection of an appropriate combination of basic components. This composite constitutes a plausible first-guess solution that increases the viability of the solution. Then, the single-scattering theory implemented in the OPAC model provides the lidar ratio.

The results show that the proposed method yields lidar ratios that agree within the uncertainty range, with both values resulting from the KFS lidar inversion and with the AERONET inversion. However, Mie theory considers that the aerosols are spherical, which, in the case of mineral dust, may lead to underestimation of the lidar ratio [6]. Therefore, in these cases, we have substituted the Mie-modeled lidar-ratio values with the computations of Dubovik *et al.* [18] for spheroid-like particle shapes. The drawback of the proposed method is that, when mineral dust is detected, the lidar-ratio value depends on the availability of the radiance inversions. In the longer term, a better solution would probably be to devise a spheroid-based scattering model to replace the spherical model currently used in OPAC.

We have obtained a climatology of the lidar ratio according to the air-mass classification. The EU sector has a median lidar ratio of 59 ± 11 sr, as it is dominated by continental aerosols (88% of occurrence). The AF sector has a median lidar ratio of 55 ± 5 sr due to a 12% occurrence of maritime pure or mixture with continental (with median lidar ratio of 43 ± 5 sr), as well as 44% of mineral dust (56% of which have a radius of 2 μm, thus with a lidar ratio of 55 sr according to Dubovik *et al.* [18]). The results for the Atlantic Ocean sections AML, AR, and TR are very similar. Maritime aerosols appeared on more than 80% of the days, leading to median lidar ratios of 36 ± 11, 31 ± 11, and 37 ± 9 sr, respectively. With regard to the mixed air-mass types, the results are considered relevant when they include at least 4% of the days. TR–AF has a median lidar ratio of 55 ± 7 sr as a result of 43% of mineral intrusions and 30% of maritime pure aerosols. In sectors TR–EU and AML–EU continental aerosols prevail, leading to median lidar ratios of 59 ± 13 and 59 ± 11 sr, respectively.

The advantage of the proposed technique to retrieve the lidar ratio is that which is based on direct-sunlight measurements. The AERONET-retrieved lidar ratios are only available when no clouds are present at all. Moreover, the radiance inversion requirements (high aerosol loading and large elevation angle) reduce further the data that can be used. Thus, the proposed method will be more applicable for practical use.

Next, a climatology of the lidar ratio only based on back trajectories will be explored. This knowledge of the lidar ratio would benefit satellite lidars GLAS and CALIPSO when ancillary data such as the AOD are not available, yet air-mass back trajectories are.

ACKNOWLEDGMENT

The authors would like to thank for the AERONET project (NASA) for the continuous effort put into the quality assurance and processing of the Sun-photometric data. The authors would also like to thank the NOAA Air Resources Laboratory for the provision of the HYSPLIT transport and dispersion model used in this paper.

REFERENCES

[1] J. Ackermann, "The extinction-to-backscatter ratio of tropospheric aerosol: A numerical study," *J. Atmos. Ocean. Technol.*, vol. 15, no. 4, pp. 1043–1050, Aug. 1998.

[2] T. L. Anderson, S. J. Masonis, D. S. Covert, R. Charlson, and M. Rood, "In situ measurement of the aerosol extinction-to-backscatter ratio at a polluted continental site," *J. Geophys. Res.*, vol. 105, no. D22, pp. 26 907–26 915, Nov. 2000.

[3] A. Ångström, "The parameters of atmospheric turbidity," *Tellus*, vol. 16, no. 1, pp. 64–76, 1964.

[4] A. Ansmann, U. Wandinger, M. Riebesell, C. Weitkamp, and W. Michaelis, "Independent measurement of extinction and backscatter profiles in cirrus clouds by using a combined Raman elastic-backscatter lidar," *Appl. Opt.*, vol. 31, no. 33, pp. 7113–7131, Nov. 1992.

[5] A. Ansmann, F. Wagner, D. Althausen, D. Müller, A. Herber, and U. Wandinger, "European pollution outbreaks during ACE 2: Lofted aerosol plumes observed with Raman lidar at the Portuguese coast," *J. Geophys. Res.*, vol. 106, no. D18, pp. 20 725–20 734, Sep. 2001.

[6] F. Barnaba and G. P. Gobbi, "Lidar estimation of tropospheric aerosol extinction, surface area and volume: Maritime and desert-dust cases," *J. Geophys. Res.*, vol. 106, no. D3, pp. 3005–3018, Feb. 2001.

[7] R. G. Barry and R. J. Chorley, *Atmosphere, Weather and Climate*, 7th ed. London, U.K.: Routledge, 1998.

[8] B. A. Bodhaine, N. B. Wood, E. G. Dutton, and J. R. Slusser, "On Rayleigh optical depth calculations," *J. Atmos. Ocean. Technol.*, vol. 16, no. 11, pp. 1854–1861, Nov. 1999.

[9] J. Bösenberg, V. Matthias, A. Amodeo, V. Amoridis, A. Ansmann, J. M. Baldasano, I. Balin, D. Balis, C. Böckmann, A. Boselli, G. Carlsson, A. Chaikovsky, G. Chourdakis, A. Comeron, F. De Tomasi, R. Eixmann, V. Freudenthaler, H. Giehl, I. Grigorov, A. Hågård, M. Iarlori, A. Kirsche, G. Kolarov, L. Komguem, S. Kreipl, W. Kumpf, G. Larchevêque, H. Linné, R. Matthey, I. Mattis, A. Mekler, I. Mironova, V. Mitev, L. Mona, D. Müller, S. Music, S. Nickovic, M. Pandolfi, A. Papayannis, G. Pappalardo, J. Pelon, C. Pérez, R. M. Perrone, R. Persson, D. P. Resendes, V. Rizi, F. Rocadenbosch, J. A. Rodrigues, L. Sauvage, L. Schneidenbach, R. Schumacher, V. Shcherbakov, V. Simeonov, P. Sobolewski, N. Spinelli, I. Stachlewska, D. Stoyanov, T. Trickl, G. Tsaknakis, G. Vaughan, U. Wandinger, X. Wang, M. Wiegner, M. Zavrtanik, and C. Zerefos, "EARLINET: A European aerosol research lidar network to establish an aerosol climatology," Max Planck Inst. Meteorol., Hamburg, Germany, Rep. 348, 2003.

[10] C. J. Bruegge, J. E. Conel, R. O. Green, J. S. Margolis, R. G. Holm, and G. Toon, "Water vapor abundance retrievals during FIFE," *J. Geophys. Res.*, vol. 97, no. D17, pp. 18 759–18 768, Nov. 1992.

[11] C. Cattrall, J. Reagan, K. Thome, and O. Dubovik, "Variability of aerosol and spectral lidar and backscatter and extinction ratios of key aerosol types derived from selected Aerosol Robotic Network locations," *J. Geophys. Res.*, vol. 110, no. D10, p. D10 S11, May 2005. DOI:10.1029/2004JD005124.

[12] P. Chazette, C. David, J. Lefrère, S. Godin, J. Pelon, and G. Mégie, "Comparative lidar study of the optical, geometrical, and dynamical properties of stratospheric post-volcanic aerosols, following the eruptions of El Chichon and Mount Pinatubo," *J. Geophys. Res.*, vol. 100, no. D11, pp. 23 195–23 207, Nov. 1995.

[13] G. A. d'Almeida, P. Koepke, and E. P. Shettle, *Atmospheric Aerosols: Global Climatology and Radiative Characteristics*. Hampton, VA: Deepak, 1991.

[14] S. J. Doherty, T. L. Anderson, and R. J. Charlson, "Measurement of the lidar ratio for atmospheric aerosols with a 180 degrees backscatter nephelometer," *Appl. Opt.*, vol. 38, no. 9, pp. 1823–1832, Mar. 1999.

[15] R. R. Draxler and G. D. Hess, "An overview of the HYSPLIT_4 modelling system for trajectories, dispersion, and deposition," *Aust. Meteorol. Mag.*, vol. 47, no. 4, pp. 295–308, Dec. 1998.

[16] O. Dubovik, A. Smirnov, B. N. Holben, M. D. King, Y. J. Kaufman, T. F. Eck, and I. Slutsker, "Accuracy assessments of aerosol optical properties retrieved from Aerosol Robotic Network (AERONET) Sun and sky radiance measurements," *J. Geophys. Res.*, vol. 105, no. D8, pp. 9791–9806, Apr. 2000.

[17] O. Dubovik, B. N. Holben, T. F. Eck, A. Smirnov, Y. J. Kaufman, M. D. King, D. Tanré, and I. Slutsker, "Variability of absorption and optical properties of key aerosol types observed in worldwide locations," *J. Atmos. Sci.*, vol. 59, no. 3, pp. 590–608, Feb. 2002.

[18] O. Dubovik, A. Sinyuk, T. Lapyonok, B. N. Holben, M. Mishchenko, P. Yang, T. F. Eck, H. Volten, O. Muñoz, B. Veihelmann, W. J. van der Zande, J.-F. Leon, M. Sorokin, and I. Slutsker, "Application of spheroid models to account for aerosol particle nonsphericity in remote sensing of desert dust," *J. Geophys. Res.*, vol. 111, no. D11, p. D11 208, Jun. 2006. DOI:10.1029/2005JD006619.

[19] T. F. Eck, B. N. Holben, J. S. Reid, O. Dubovik, A. Smirnov, N. T. O'Neill, I. Slutsker, and S. Kinne, "Wavelength dependence of the optical depth of biomass burning, urban, and desert dust aerosols," *J. Geophys. Res.*, vol. 104, no. D24, pp. 31 333–31 349, Dec. 1999.

[20] V. Estellés, M. P. Utrillas, J. A. Martínez-Lozano, A. Alcántara, L. Alados-Arboledas, F. J. Olmo, J. Lorente, X. de Cabo, V. Cachorro, H. Horvath, A. Labajo, M. Sorribas, J. P. Díaz, A. M. Díaz, A. M. Silva, T. Elías, M. Pujadas, J. A. Rodrigues, J. Cañada, and Y. García, "Intercomparison of spectroradiometers and Sun photometers for the determination of the aerosol optical depth during the VELETA-2002 field campaign," *J. Geophys. Res.*, vol. 111, no. D17, p. D17 207, Sep. 2006. DOI:10.1029/2005JD006047.

[21] V. Estellés, J. A. Martínez-Lozano, M. P. Utrillas, and M. Campanelli, "Columnar aerosol properties in Valencia (Spain) by ground-based sun photometry," *J. Geophys. Res.*, vol. 112, no. D11, p. D11 201, Jun. 2007. DOI:10.1029/2006JD008167.

[22] V. Estellés, J. A. Martínez-Lozano, and M. P. Utrillas, "Influence of air mass history on the columnar aerosol properties at Valencia, Spain," *J. Geophys. Res.*, vol. 112, no. D15, p. D15 211, Aug. 2007. DOI: 10.1029/2007JD008593.

[23] F. G. Fernald, "Analysis of atmospheric lidar observation—Some comments," *Appl. Opt.*, vol. 23, no. 5, pp. 652–653, Mar. 1984.

[24] C. Flamant, J.-P. Chaboureau, D. J. Parker, C. M. Taylor, J.-P. Cammas, O. Bock, F. Timouk, and J. Pelon, "Airborne observations of the impact of a convective system on the planetary boundary layer thermodynamics and aerosol distribution in the inter-tropical discontinuity region of the West African Monsoon," *Q. J. R. Meteorol. Soc.*, vol. 133, no. 626, pp. 1175–1189, Jul. 2007.

[25] K. Franke, A. Ansmann, D. Müller, D. Althausen, F. Wagner, and R. Scheele, "One-year observations of particle lidar ratio over the tropical Indian Ocean with Raman lidar," *Geophys. Res. Lett.*, vol. 28, no. 24, pp. 4559–4562, Dec. 2001.

[26] G. P. Gobbi, "Lidar estimation of stratospheric aerosol properties: Surface, volume, and extinction to backscatter ratio," *J. Geophys. Res.*, vol. 100, no. D6, pp. 11 219–11 236, Jun. 1995.

[27] C. A. Gueymard, "Parameterized transmittance model for direct beam and circumsolar spectral irradiance," *Sol. Energy*, vol. 71, no. 5, pp. 325–346, Nov. 2001.

[28] G. Haenel, "The properties of atmospheric aerosol particles as a function of the relative humidity at thermodynamic equilibrium with the scattering moist air," *Adv. Geophys.*, vol. 19, pp. 73–188, 1976.

[29] C. L. Heald, D. J. Jacob, S. Turquety, R. C. Hudman, R. J. Weber, A. P. Sullivan, R. E. Peltier, E. L. Atlas, J. A. de Gouw, C. Warneke, J. S. Holloway, J. A. Neuman, F. M. Flocke, and J. H. Seinfeld, "Concentrations and sources of organic carbon aerosols in the free troposphere over North America," *J. Geophys. Res.*, vol. 111, no. D23, p. D23 S47, 2006. DOI: 10.1029/2006JD007705.

[30] J. W. Hair, C. A. Hostetler, A. L. Cook, D. B. Harper, R. A. Ferrare, T. L. Mack, W. Welch, L. R. Izquierdo, and F. E. Hovis, "Airborne high spectral resolution lidar for profiling aerosol optical properties," *Appl. Opt.*, vol. 47, no. 36, pp. 6734–6752, Dec. 2008.

[31] J. Hansen, M. Sato, and R. Ruedy, "Radiative forcing and climate response," *J. Geophys. Res.*, vol. 102, no. D6, pp. 6831–6864, 1997.

[32] J. Haywood and O. Boucher, "Estimates of the direct and indirect radiative forcing due to tropospheric aerosols: A review," *Rev. Geophys.*, vol. 38, no. 4, pp. 513–543, 2000.

[33] M. Hess, P. Koepke, and I. Schult, "Optical properties of aerosols and clouds: The software package OPAC," *Bull. Amer. Meteorol. Soc.*, vol. 79, no. 5, pp. 831–844, May 1998.

[34] B. N. Holben, T. F. Eck, I. Slutsker, D. Tanré, J. P. Buis, A. Setzer, E. Vermote, J. A. Reagan, Y. J. Kaufman, T. Nakajima, F. Lavenu, I. Jankowiak, and A. Smirnov, "AERONET—A federated instrument network and data archive for aerosol characterization," *Remote Sens. Environ.*, vol. 66, no. 1, pp. 1–16, Oct. 1998.

[35] B. N. Holben, D. Tanré, A. Smirnov, T. F. Eck, I. Slutsker, N. Abuhassan, W. W. Newcomb, J. S. Schafer, B. Chatenet, F. Lavenu, Y. J. Kaufman, J. Vande Castle, A. Setzer, B. Markham, D. Clark, R. Frouin, R. Halthore, A. Karneli, N. T. O'Neill, C. Pietras, R. T. Pinker, K. Voss, and G. Zibordi, "An emerging ground-based aerosol climatology: Aerosol optical depth from AERONET," *J. Geophys. Res.*, vol. 106, no. D11, pp. 12 067–12 097, Jun. 2001.

[36] T. Holzer-Popp, M. Schroedter, and G. Gesell, "Retrieving aerosol optical depth and type in the boundary layer over land and ocean from simultaneous GOME spectrometer and ATSR-2 radiometer measurements, 1, Method description," *J. Geophys. Res.*, vol. 107, no. D21, pp. AA C16-1–AA C16-17, Dec. 2002.

[37] R. B. Husar, D. M. Tratt, B. A. Schichtel, S. R. Falke, F. Li, D. Jaffe, S. Gassó, T. Gill, N. S. Laulainen, F. Lu, M. C. Reheis, Y. Chun, D. Westphal, B. N. Holben, C. Gueymard, I. McKendry, N. Kuring, G. C. Feldman, C. McClain, R. J. Frouin, J. Merrill, D. DuBois, F. Vignola, T. Murayama, S. Nickovic, W. E. Wilson, K. Sassen, N. Sugimoto, and W. C. Malm, "Asian dust events of April 1998," *J. Geophys. Res.*, vol. 106, no. D16, pp. 18 317–18 330, Aug. 2001.

[38] H. Jäger, "Long-term record of lidar observations of the stratospheric aerosol layer at Garmisch–Partenkirchen," *J. Geophys. Res.*, vol. 110, no. D8, p. D08 106, Apr. 2005. DOI: 10.1029/2004JD005506.

[39] J. D. Klett, "Lidar inversion with variable backscatter extinction ratios," *Appl. Opt.*, vol. 24, no. 11, pp. 1638–1643, Jun. 1985.

[40] V. A. Kovalev, "Sensitivity of the lidar solution to errors of the aerosol backscatter-to-extension ratio: Influence coefficient," *Appl. Opt.*, vol. 34, no. 18, pp. 3457–3462, Jun. 1995.

[41] Z. Y. Liu, N. Sugimoto, and T. Murayama, "Extinction-to-backscatter ratio of Asian dust observed with high-spectral-resolution lidar and Raman lidar," *Appl. Opt.*, vol. 41, no. 9, pp. 2760–2767, Mar. 2002.

[42] F. Marenco, V. Santacesaria, A. F. Bais, U. Balis, A. di Sarra, A. Papayannis, and C. Zerefos, "Optical properties of tropospheric aerosols determined by lidar and spectrophotometric measurements Photochemical Activity and Solar Ultraviolet Radiation campaign," *Appl. Opt.*, vol. 36, no. 27, pp. 6875–6886, Sep. 1997.

[43] J. A. Martínez-Lozano, M. P. Utrillas, F. Tena, and V. Cachorro, "The parameterisation of the atmospheric aerosol optical depth using the Angstrom power law," *Sol. Energy*, vol. 63, no. 5, pp. 303–311, Nov. 1998.

[44] S. J. Masonis, "An empirical study of the lidar ratio and its variability, with implications for determining climate forcing by satellite-borne lidar," Ph.D. dissertation, Univ. Washington Press, Seattle, WA, 2001.

[45] V. Matthias and J. Bösenberg, "Aerosol climatology for the planetary boundary layer derived from regular lidar measurements," *Atmos. Res.*, vol. 63, no. 3/4, pp. 221–245, Aug. 2002.

[46] I. Mattis, A. Ansmann, D. Müller, U. Wandinger, and D. Althausen, "Dual-wavelength Raman lidar observations of the extinction-to-backscatter ratio of Saharan dust," *Geophys. Res. Lett.*, vol. 29, no. 9, pp. 20.1–20.4, May 2002.

[47] M. J. McGill, M. A. Vaughan, C. R. Trepte, W. D. Hart, D. L. Hlavka, D. M. Winker, and R. Kuehn, "Airborne validation of spatial properties measured by the CALIPSO lidar," *J. Geophys. Res.*, vol. 112, no. D20, p. D20 201, Oct. 2007. DOI:10.1029/2007JD008768.

[48] M. Mishchenko, L. Travis, R. Kahn, and R. West, "Modeling phase functions for dustlike tropospheric aerosols using a shape mixture of randomly oriented polydisperse spheroids," *J. Geophys. Res.*, vol. 102, no. D14, pp. 16 831–16 847, Jul. 1997.

[49] M. Morys, F. M. Mims, III, S. Hagerup, S. E. Anderson, A. Baker, J. Kia, and T. Walkup, "Design, calibration, and performance of MICROTOPS II handheld ozone monitor and Sun photometer," *J. Geophys. Res.*, vol. 106, no. D13, pp. 14573–14582, Jul. 2001.

[50] D. Müller, A. Ansmann, I. Mattis, M. Tesche, U. Wandinger, D. Althausen, and G. Pisani, "Aerosol-type-dependent lidar ratios observed with Raman lidar," *J. Geophys. Res.*, vol. 112, no. D16, p. D16 202, Aug. 2007. DOI:10.1029/2006JD008292.

[51] T. Nakajima, G. Tonna, R. Rao, P. Boi, Y. Kaufman, and B. Holben, "Use of sky brightness measurements from ground for remote sensing of particulate polydispersions," *Appl. Opt.*, vol. 35, no. 15, pp. 2672–2686, 1996.

[52] A. Nelder and R. Mead, "A simplex method for function minimization," *Comput. J.*, vol. 7, no. 4, pp. 308–313, 1965.

[53] K. Niranjan, V. Sreekanth, B. L. Madhavan, and K. Krishna Moorthy, "Aerosol physical properties and Radiative forcing at the outflow region from the Indo-Gangetic plains during typical clear and hazy periods of wintertime," *Geophys. Res. Lett.*, vol. 34, no. 19, p. L19 805, Oct. 2007. DOI:10.1029/2007GL031224.

[54] T. Novakov and J. E. Penner, "Large contribution of organic aerosols to cloud-condensation-nuclei concentrations," *Nature*, vol. 365, no. 6449, pp. 823–826, Oct. 1993.

[55] J. Pelon, C. Flamant, P. Chazette, J.-F. Leon, D. Tanre, M. Sicard, and S. K. Satheesh, "Characterization of aerosol spatial distribution and optical properties over the Indian Ocean from airborne LIDAR and radiometry during INDOEX'99," *J. Geophys. Res.*, vol. 107, no. D19, p. 8029, Sep./Oct. 2002. DOI:10.1029/2001JD000402.

[56] F. Raes, R. Van Dingenen, E. Vignati, J. Wilson, J.-P. Putaud, J. H. Seinfeld, and P. Adams, "Formation and cycling of aerosols in the global troposphere," *Atmos. Environ.*, vol. 34, no. 25, pp. 4215–4240, Jul. 2000.

[57] F. Rocadenbosch and A. Comeron, "Error analysis for the lidar backward inversion algorithm," *Appl. Opt.*, vol. 38, no. 21, pp. 4461–4474, Jul. 1999.

[58] F. Rocadenbosch, M. Sicard, A. Comerón, J. M. Baldasano, A. Rodríguez, R. Agishev, C. Muñoz, M. A. López, and D. García-Vizcaino, "The UPC scanning Raman lidar: An engineering overview," in *Proc. 21st ILRC*, 2002, vol. 1, pp. 69–70.

[59] Y. Sasano and H. Nakane, "Significance of the extinction/backscatter ratio and the boundary value term in the solution for the two-component lidar equation," *Appl. Opt.*, vol. 23, no. 1, pp. 11–13, Jan. 1984.

[60] Y. Sasano, E. V. Browell, and S. Ismail, "Error caused by using a constant extinction backscattering ratio in the lidar solution," *Appl. Opt.*, vol. 24, no. 22, pp. 3929–3932, Nov. 1985.

[61] J. J. Seinfeld and S. N. Pandis, *Atmospheric Chemistry and Physics, From Air Pollution to Climate Change*. Hoboken, NJ: Wiley, 2006, ch. 8, pp. 388–389.

[62] M. Sicard, C. Pérez, F. Rocadenbosch, J. M. Baldasano, and D. García-Vizcaino, "Mixed-layer depth determination in the Barcelona coastal area from regular lidar measurements: Methods, results and limitations," *Bound.-Layer Meteorol.*, vol. 119, no. 1, pp. 135–157, Apr. 2006.

[63] A. Smirnov, B. N. Holben, I. Slutsker, E. Welton, and P. Formenti, "Optical properties of Saharan dust during ACE 2," *J. Geophys. Res.*, vol. 103, no. D21, pp. 28 079–28 092, Nov. 1998.

[64] A. Smirnov, B. N. Holben, T. F. Eck, O. Dubovik, and I. Slutsker, "Cloud screening and quality control algorithms for the AERONET database," *Remote Sens. Environ.*, vol. 73, no. 3, pp. 337–349, Sep. 2000.

[65] A. Smirnov, B. N. Holben, Y. J. Kaufman, O. Dubovik, T. F. Eck, I. Slutsker, C. Pietras, and R. Halthore, "Optical properties of atmospheric aerosol in maritime environments," *J. Atmos. Sci.*, vol. 59, no. 3, pp. 501–523, Feb. 2002.

[66] E. P. Shettle and R. W. Fenn, "Models for the aerosols of the lower atmosphere and the effects of humidity variations on their optical properties," Air Force Geophys. Lab., Bedford, MA, AFGL-TR-79-0214, 1979. Environmental Research Papers, no. 676.

[67] J. D. Spinhirne, J. A. Reagan, and B. M. Herman, "Vertical distribution of aerosol extinction cross section and inference of aerosol imaginary index in the troposphere by lidar technique," *J. Appl. Meteorol.*, vol. 19, no. 4, pp. 426–438, Apr. 1980.

[68] J. D. Spinhirne, S. P. Palm, W. D. Hart, D. L. Hlavka, and E. J. Welton, "Cloud and aerosol measurements from GLAS: Overview and initial results," *Geophys. Res. Lett.*, vol. 32, no. 22, p. L22 S03, Sep. 2005. DOI:10.1029/2005GL023507.

[69] *U.S. Standard Atmosphere*, U.S. Gov. Printing Office, Washington, DC, 1976.

[70] P. Stier, J. Feichter, S. Kinne, S. Kloster, E. Vignati, J. Wilson, L. Ganzeveld, I. Tegen, M. Werner, Y. Balkanski, M. Schulz, O. Boucher, A. Minikin, and A. Petzold, "The aerosol-climate model ECHAM5-HAM," *Atmos. Chem. Phys.*, vol. 5, pp. 1125–1156, Mar. 2005.

[71] T. Takamura and T. Nakajima, "Overview of SKYNET and its activities," *Opt. Pura Apl.*, vol. 37, no. 3, pp. 3303–3308, 2004.

[72] D. Winker, W. Hunt, and M. McGill, "Initial performance assessment of CALIOP," *Geophys. Res. Lett.*, vol. 34, no. 19, p. L19 803, Oct. 2007. DOI:10.1029/2007GL030135.

[73] *AERONET Website*, 2009, Goddard Space Flight Center, NASA. [Online]. Available: http://aeronet.gsfc.nasa.gov/new_web/index.html

[74] *ECMWF Homepage*, 2009. [Online]. Available: http://www.ecmwf.int

[75] *HYSPLIT Dispersion Model Website*, 2009, Air Resources Laboratory, National Oceanic and Atmospheric Administration. [Online]. Available: http://www.arl.noaa.gov/ready/hysplit4.html

[76] *TOMS Website*, 2009, NASA. [Online]. Available: http://jwocky.gsfc.nasa.gov

Roberto Pedrós received the M.Sc. and Ph.D. degrees from the University of Valencia, Valencia, Spain, in 1997 and 2002, respectively.

He is currently an Associate Professor with the Department of Earth Physics, University of Valencia. He works with the Solar Radiation Group since 1995. His research interest is better knowledge of the impact of atmospheric aerosols on climate.

Víctor Estellés received the B.Sc., M.Sc., and Ph.D. degrees in physics from the University of Valencia, Valencia, Spain, in 1999, 2003, and 2006, respectively.

Since 2001, he has been with the Solar Radiation Group, Department of Earth Physics, University of Valencia, where his main field of interest aims at Sun photometry, which is related to the characterization of atmospheric aerosols. His current interests have broaded to the study of radiative forcing of aerosols and the development of the European SKYRAD user network.

Michaël Sicard received the M.Sc. and Ph.D. degrees in physical methods for remote sensing from the Service d'Aéronomie, Institut Pierre-Simon Laplace, Paris, France, in 1995 and 2000, respectively.

He is currently an Associate Professor with the Department of Signal Theory and Communications, Polytechnic University of Catalonia, Barcelona, Spain, where he is also with the Remote Sensing Laboratory. His main research interest is twofold: 1) on a technical point of view, the development of lidar techniques and instruments in all their aspects for aerosol observations and 2) the study of aerosols. The latter includes aerosol optical and microphysical characterization due to data fusion, aerosol transport, and atmospheric-boundary-layer study and modeling. He is a Coordinator of the Spanish/Portuguese aerosol lidar network.

José Luis Gómez-Amo received the M.Sc. degree in physics and the Ph.D. degree in environmental physics and thermodynamics from the University of Valencia, Valencia, Spain, in 1999 and 2006, respectively.

He is currently with the Solar Radiation Group, Department of Earth Physics, University of Valencia. His main research has been focused on the study of the optical properties of atmospheric aerosols and their implications on climate. His research interest also includes the study of solar-energy systems and energy-saving analysis.

María Pilar Utrillas received the M.Sc. and Ph.D. degrees from the University of Valencia, Valencia, Spain, in 1989 and 1995, respectively.

She is currently with the Solar Radiation Group, Department of Earth Physics, University of Valencia, where she has specialized in radiation-transfer codes and in solar spectral and integral instrumentation and is teaching mainly physics and atmospheric radiative transfer. Her main investigation work has been focused in the study and analysis of atmospheric aerosols and their influence on solar radiation reaching the Earth's surface.

José A. Martínez-Lozano received the M.Sc. and Ph.D. degrees in physics from the University of Valencia, Valencia, Spain, in 1975 and 1983, respectively.

He is currently with the Department of Earth Physics, University of Valencia, where he teaches, among other subjects, physics, has specialized in atmospheric radiative transfer, and is directing the Solar Radiation Group. One of the main interests of the group consists of the validation of satellite measurements employing sensors on the Earth surface. Since the beginning, he has been developing his research work in the area of solar radiation, considering initially integrated values and studying the spectral ones lately. His current main efforts are oriented mainly to the study of the optical properties of atmospheric aerosols.

F. Rocadenbosch, photograph and biography not available at the time of publication.

C. Pérez, photograph and biography not available at the time of publication.

José María Baldasano Recio received the M.Sc. and Ph.D. degrees in chemistry from the University of Barcelona, Barcelona, Spain, in 1973 and 1983, respectively, and the Chemical Engineer degree from the Institut National Polytechnique de Toulouse, Toulouse, France, in 1979.

He is currently a Full Professor in environmental engineering with the Earth Sciences Department, Polytechnic University of Catalonia, Barcelona, Spain, where he is also the Head of the Barcelona Supercomputing Center. His research activities are oriented to air quality and climate modeling. He is the author of more than 240 publications in scientific and technical journals, and more than 135 communications and 120 reports in congresses and 60 conferences, and is the coeditor and author of 14 books in environmental topics. He is the Cochairman of five environmental international conferences and has been an Advisor of more 80 companies and administrations.

Prof. Baldasano Recio was the recipient of the "Rey Jaime I" Award in Environmental Protection in 1997. He is a member of the Intergovernmental Panel on Climate Change.